

Articles

X-ray Snapshot of the Mechanism of Inactivation of Human Neutrophil Elastase by 1,2,5-Thiadiazolidin-3-one 1,1-Dioxide Derivatives[†]

Weijun Huang,[§] Yasufumi Yamamoto,[§] Yi Li,[‡] Dengfeng Dou,[‡] Kevin R. Alliston,[‡] Robert P. Hanzlik,[§] Todd D. Williams,^{||} and William C. Groutas^{*‡}

Department of Chemistry, Wichita State University, Wichita, Kansas 67260, Protein Structure Laboratory, The University of Kansas, Lawrence, Kansas 66047, and Mass Spectrometry Lab, The University of Kansas, Lawrence, Kansas 66047

Received August 2, 2007

The mechanism of action of a general class of mechanism-based inhibitors of serine proteases, including human neutrophil elastase (HNE), has been elucidated by determining the X-ray crystal structure of an enzyme–inhibitor complex. The captured intermediate indicates that processing of inhibitor by the enzyme generates an N-sulfonyl imine functionality that is tethered to Ser195, in accordance with the postulated mechanism of action of this class of inhibitors. The identity of the HNE-N-sulfonyl imine species was further corroborated using electrospray ionization mass spectrometry.

Introduction

Mechanism-based (suicide) inhibitors have been extensively used in mechanistic enzymology, and drug design and discovery.¹ Indeed, several drugs currently in the clinic exert their effects by utilizing a mechanism-based type of inhibition. A mechanism-based inhibitor is typically a molecule of low reactivity that acts as a substrate and is processed by the catalytic machinery of an enzyme, generating a reactive electrophilic species while tethered to the active site. Subsequent reaction with an active site nucleophilic residue leads to irreversible inactivation of the enzyme. A noteworthy advantage of this type of inhibitor is its potentially high enzyme selectivity because the latent electrophilic species is unmasked following catalytic processing of the inhibitor by the target enzyme only.

A major focus of our research has been the design of mechanism-based inhibitors of proteases, in particular, serine proteases believed to be involved in chronic obstructive pulmonary disease (COPD) and related inflammatory ailments.² We have recently described the structure-based design of the 1,2,5-thiadiazolidin-3-one 1,1-dioxide scaffold (**I**; Figure 1) and its subsequent utilization in the design of mechanism-based inhibitors of chymotrypsin-like serine proteases. Specifically, we have demonstrated that compounds represented by structure **I**, where L is an appropriate leaving group, function as potent, time-dependent, irreversible inhibitors of human neutrophil elastase (HNE^a) and related serine proteases.³ It was also established that inhibitory potency is dependent not only on the pK_a of the leaving group but also on its inherent structure, namely, the structure of L can be tweaked to enhance binding affinity through favorable interactions with the S' subsites.^{4,5}

* To whom correspondence should be addressed. Tel.: (316) 978 7374. Fax: (316) 978 3431. E-mail: bill.groutas@wichita.edu.

[§] Protein Structure Laboratory, The University of Kansas.

[‡] Wichita State University.

^{||} Mass Spectrometry Lab, The University of Kansas.

[†] Coordinates of the HNE-inhibitor(**I**) complex have been deposited in the Protein Data Bank with the access code of 2RG3.

^a Abbreviations: HNE, human neutrophil elastase; COPD, chronic obstructive pulmonary disease; PR 3, proteinase 3.

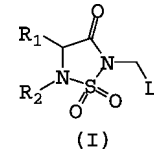


Figure 1. General structure of inhibitor **I**.

More importantly, structure **I** constitutes a *general* class of mechanism-based inhibitors, which docks to the active site in a substrate-like fashion, with R₁ occupying the primary specificity subsite S₁. Consequently, the nature of R₁ determines which subclass of serine proteases (neutral, basic, acidic) will be inhibited.⁶ Thus, optimal selectivity can be attained by varying the nature of R₁ and exploiting differences in the S' subsites of the target enzymes.

Experimental evidence in support of the postulated mechanism of action of **I** (Figure 2) rested on the isolation and characterization of low molecular products arising from the turnover of **I** by the enzyme because initial attempts to obtain an X-ray crystal of the enzyme–inhibitor complex were unsuccessful. We describe herein the results of biochemical, X-ray crystallographic, and ESI-MS studies in support of the mechanism of action (Figure 2) of this class of mechanism-based inhibitors.

Results and Discussion

Inhibitor Design Rationale. COPD involves the interplay of a range of proteolytic enzymes, including human neutrophil elastase (HNE) and proteinase 3 (PR 3). HNE and PR 3 have the ability to degrade lung elastin, the major component of lung connective tissue, and basement membrane components.⁷ HNE is a basic, 218 amino acid single polypeptide glycoprotein (M_r 29500) whose primary structure shows considerable homology (54%) with PR 3. Several X-ray crystal structures of HNE complexed to low molecular weight or protein inhibitors are available.⁸ The X-ray crystal structure of PR 3 by itself has also been determined.⁹ These structures, as well as biochemical studies aimed at mapping the active site of these enzymes using

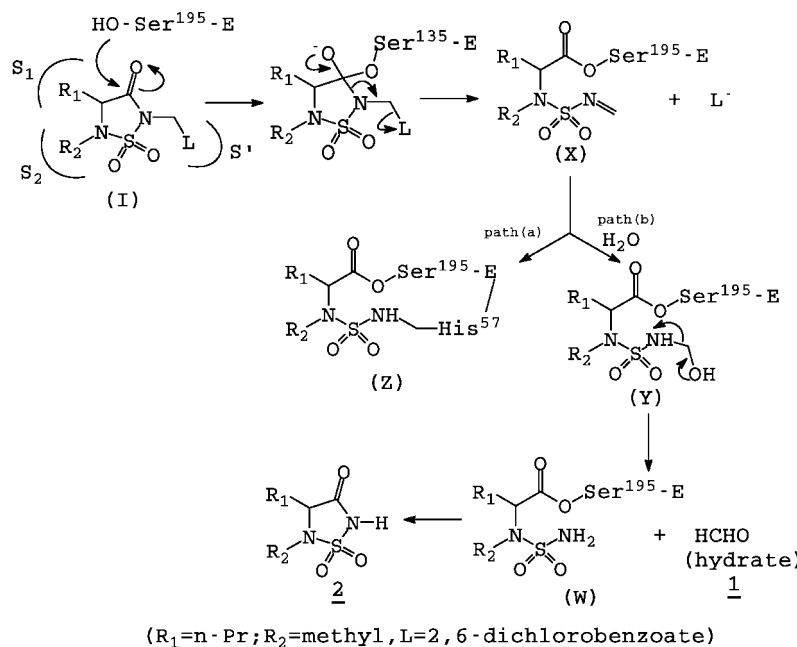


Figure 2. Postulated mechanism of action of inhibitor **I**.

peptidyl *p*-nitroanilide or peptidyl thiobenzyl substrates,^{10–13} have established that the two enzymes have extended binding sites and show a strong preference for small hydrophobic P1 residues, such as isopropyl, *n*-propyl, and isobutyl for HNE and ethyl or *n*-propyl for PR 3. Because we desired inhibitor **I** to inhibit both enzymes, R₁ = *n*-propyl was chosen as the P1 residue. Furthermore, the selection of R₂ = methyl was based on previous studies, which have shown that the nature of R₂ has a profound effect on the stability of the resulting enzyme–inhibitor acyl complex(es), and that optimal stability is attained when R₂ = methyl.³ Lastly, the selection of a carboxylate leaving group was based on the superior inhibitory prowess bestowed upon this class of inhibitors by this particular moiety and their demonstrated effectiveness in blocking the degradative action of HNE on elastin *in vitro*.^{3d}

Synthesis. Inhibitor **I** (R₁ = *n*-propyl, R₂ = methyl, L = 2,6-dichlorobenzoate) was readily synthesized starting with L-norvaline methyl ester using previously described methodology.^{3d}

Biochemical Studies. Incubation of inhibitor **I** with HNE led to rapid, time-dependent, irreversible loss of enzymatic activity (Figure 3). The bimolecular rate constant k_{inact}/K_1 , an index of inhibitor potency, was determined using the progress curve method¹⁴ and found to be $8.9 \times 10^6 \text{ M}^{-1} \text{ s}^{-1}$ (Figure 4). The k_{on} and k_{off} values were $24290 \text{ M}^{-1} \text{ s}^{-1}$ and $1.33 \times 10^{-4} \text{ s}^{-1}$, respectively, yielding an apparent inhibition constant (K_1) of 5.47 nM.^{14c} These values compare very favorably with “gold standard” inhibitors of HNE reported in the literature.¹⁵ Compound **I** was also found to inhibit human leukocyte proteinase 3 ($k_{\text{obs}}/[I]$ $3020 \text{ M}^{-1} \text{ s}^{-1}$), however, it was devoid of any inhibitory activity toward human leukocyte cathepsin G and human thrombin at an [I]/[E] ratio of 250 and a 30 min incubation time. Interestingly, incubation of **I** with bovine trypsin led to time-dependent inactivation of the enzyme despite the absence of a basic P1 residue in the inhibitor.

X-ray Crystallographic Studies/Mechanism of Action of **I.** The precise mechanism of action of this class of mechanism-based serine protease inhibitors has been in question due to a lack of relevant structural information. Although earlier studies^{3a} using a ¹³C-labeled derivative of **I** (R₁ = benzyl, R₂ = methyl,

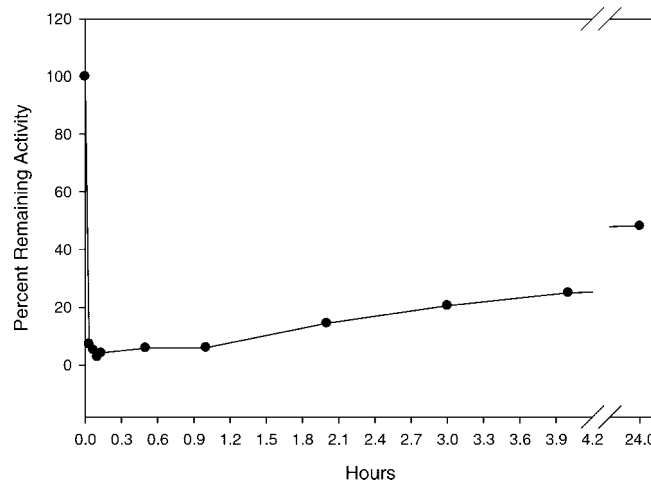


Figure 3. Time-dependent loss of enzymatic activity. Percent remaining activity versus time plot obtained by incubating inhibitor **I** (700 nM) with human neutrophil elastase (700 nM) in 0.1 M HEPES buffer containing 0.5 M NaCl, pH 7.25, and 1% DMSO. Aliquots were withdrawn at different time intervals and assayed for enzymatic activity using MeOSuc-AAPV p-NA by monitoring the absorbance at 410 nm.

L = SO₂Ph) led to the isolation and characterization of two low molecular weight products **1** and **2** (R₁ = isobutyl, R₂ = methyl), which suggested that path b (Figure 2) was operative, definitive evidence in support of the mechanism shown in Figure 2 was lacking. Thus, a crystal structure of a derivative of **I** with human neutrophil elastase was obtained to determine its mode of binding and to establish unequivocally the mechanism of action of **I**. It was initially envisioned that the structure of the enzyme–inhibitor complex would reveal whether formation of intermediate **X** would subsequently lead to enzyme–inhibitor complex **Z** via Michael addition of the imidazole of His57 to the sulfonyl imine conjugated system in **X** (“double hit” mechanism) or whether **X** would undergo Michael addition with water to yield species **Y** that then collapses to form acyl enzyme **W**.

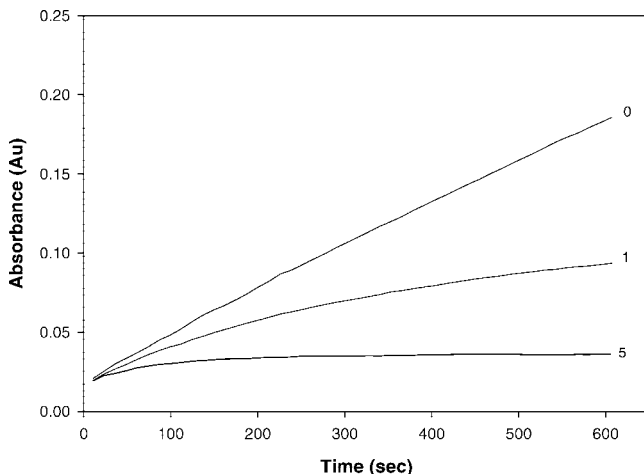


Figure 4. Progress curves for the inhibition of human neutrophil elastase (HNE) by inhibitor **I**. Absorbance was monitored at 410 nm for reaction solutions containing 10 nM HNE, 105 μ M MeOSuc-AAPV *p*-nitroanilide, and the inhibitor at the indicated inhibitor to enzyme ratios in 0.1 M HEPES buffer containing 0.5 M NaCl, pH 7.25, and 2.5% DMSO. The temperature was maintained at 25 °C, and reactions were initiated by the addition of enzyme.

Quite unexpectedly the X-ray crystal structure obtained by soaking crystals of HNE with inhibitor **I** ($R_1 = n$ -propyl, $R_2 =$ methyl, $L = 2,6$ -dichlorobenzoate) was determined to be that of intermediate **X** (Figure 5). The enzyme–inhibitor complex shows the oxygen of the active site serine (Ser195) to be covalently bound to the carbonyl carbon of the inhibitor. The distance of the sp^2 -hybridized carbon to the nearest imidazole nitrogen of His57 is 3.577 Å, which is too far to be covalently bonded to the carbon, ruling out species **Z**. Figure 5 also shows that the 2,6-dichlorobenzoate group is absent in the enzyme–inhibitor complex in accordance with the proposed mechanism of action (Figure 2). The hydrophobic *n*-propyl group occupies a pocket (S_1) formed by the main chains of Phe192 and Phe215, and the side chains of Val190, Val216, and Phe192, with which it engages in multiple hydrophobic interactions. The $SO_2NH = CH_2$ is located between the side chains of His57 and Phe192 with one of the oxygen atoms forming a hydrogen bond with His57. A surface representation of the HNE active site cleft with the docked inhibitor is shown in Figure 6. Interestingly, when crystals of complex **X** were re-examined after a significant time lapse, the modified inhibitor was found to be no longer bound to the enzyme. Specifically, the inhibitor had been completely “processed” by the enzyme. This indicates that the

interaction of **I** with HNE proceeds through multiple states of inactivated enzyme complexes that have variable stability. This is consistent with previous observations,^{3a} where the addition of excess hydroxylamine to the totally inactivated HNE–inhibitor **I** ($R_1 =$ isobutyl, $R_2 =$ methyl, $L = SO_2Ph$) adducts lead to incomplete regain in enzymatic activity.

The nature of species **X** was further probed using ESI-MS. The mass spectra of a sample of unreacted HNE and the HNE–inhibitor **I** ($R_1 = n$ -propyl, $R_2 =$ methyl, $L = 2,6$ -dichlorobenzoate) derived complex are shown in Figure 7. The mass spectrum of unreacted HNE shows two major peaks at 24522.2 and 25195.7,¹⁶ while the HNE–**I** complex shows an increase in mass of the two major components of 204 amu. The ESI-MS data support the conclusion, based on the X-ray structure, that the inhibited form of the enzyme is structure **X** and not structure **Y**, which would require a mass shift of 222.

Taken together, the available data indicate that inhibitor **I** inactivates HNE via a mechanism that involves the initial formation of a relatively stable acyl enzyme that incorporates in its structure a conjugated sulfonyl imine functionality. Subsequent slow reaction with water leads to the formation of one or more acyl enzymes of variable stability (i.e., structures **Y** and **W**) that eventually hydrolyze to regenerate active enzyme, as well as some low molecular weight products.

Experimental Section

X-ray Crystallographic Studies. Preparation of the Protein and Inhibitor. Human neutrophil elastase was purchased from Elastin Products Company, Inc., Owensville, MO. The protein powder was dissolved in 20 mM TRIS buffer, pH = 8.0 to a concentration of 15 mg/mL containing 10 mM of inhibitor.

Crystallization Conditions. The protein solution was centrifuged at 14000 g for minutes before being used for crystallization experiments. The hanging drop vapor diffusion method was employed, mixing 2 μ L of the protein solution with 2 μ L of the reservoir solution and incubated at 20 °C. Commercial kits Wizard I and Wizard II from Emerald Biosystems (www.emeraldsystems.com) were used for screening crystallization conditions. Diffraction quality crystals were found in 0.1 M HEPES, pH = 7.5, and 20% PEG8000. These crystals have a maximum size of 0.5 \times 0.1 \times 0.1 mm.

Data Collection and Structural Refinement. One crystal was soaked in 0.1 M HEPES, pH = 7.5, and 35% PEG8000 containing 10 mM inhibitor for two days before data collection was carried out. Crystals were analyzed with an R-AXIS IV++ imaging-plate detector mounted on a Rigaku RUH3R rotating-anode generator operated at 50 kV and 100 mA. Images were collected over 180 degrees in 0.5 increments at 100 K. The data was processed with HKL2000.¹⁷ The space group of the crystal belongs to $P6_3$, and

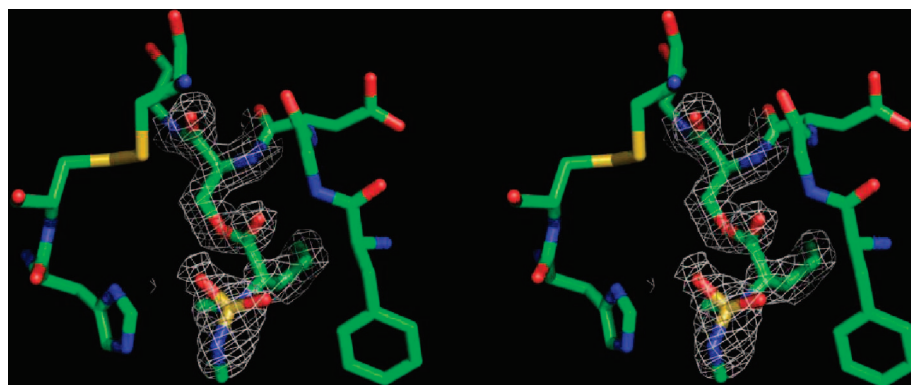


Figure 5. Stereoview of the active site region in an omit $F_o - F_c$ map of the refined protein–inhibitor complex, where the inhibitor and Ser 195 have been excluded from the structure factor calculation. The map was contoured at 3.0 times the standard deviation. Parts of the refined structure are included. The carbonyl carbon of modified inhibitor **I** is shown to be covalently bound to the Oy of Ser195.

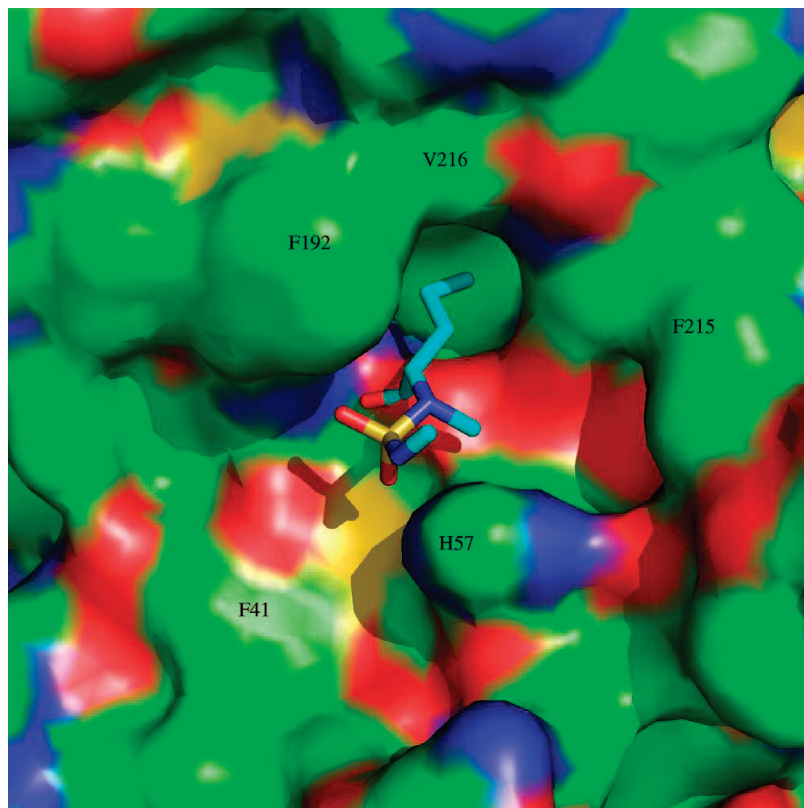


Figure 6. Three-dimensional surface of the active site of HNE with modified inhibitor **I** bound to the active site cleft and the *n*-propyl group nested into the S1 subsite.

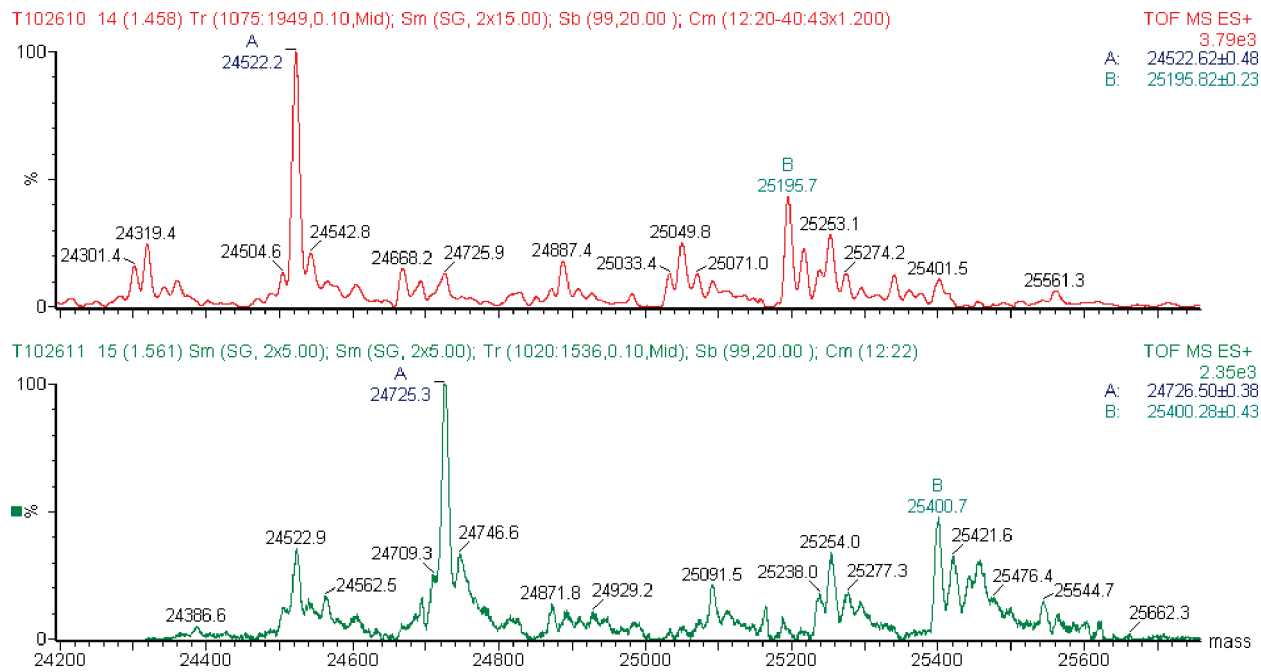


Figure 7. (a) Derived mass spectrum of HNE (top). (b) Derived mass spectrum of the HNE–inhibitor complex (bottom).

the cell dimensions were $a = b = 73.2 \text{ \AA}$, $c = 70.1 \text{ \AA}$, $\alpha = \beta = 90^\circ$, and $\gamma = 120^\circ$. A data set to 1.8 \AA resolution and 95.6% completeness was collected (Table 1).

Molecular replacement was carried out with Phaser¹⁸ using the human neutrophil elastase in complex with MeO-Suc-Ala-Ala-Pro-Val chloromethyl ketone inhibitor (1PPG) as search model. A solution with reasonable three-dimensional packing was found. Model building was carried out using O19 and crystallographic refinement was performed using CNS.²⁰ The refinement was

monitored with the free R factor throughout the whole refinement process, with 3% of the total number of reflections set aside. The initial crystallographic R factors were around 0.34, and the refinement process included simulated annealing to a starting temperature of 4000 K, positional refinement, individual B-factor refinement, and addition of water molecules. The inhibitor was modeled using O according to the electron densities shown in $2F_{\text{obs}} - F_{\text{calc}}$ and $F_{\text{obs}} - F_{\text{calc}}$ maps. These electron-density maps were examined with different contour levels. The $2F_{\text{obs}} - F_{\text{calc}}$ map was

Table 1. X-ray Diffraction Data Collection and Refinement Statistics

Data Statistics	
resolution	50–1.8 (1.80–1.86)
collected reflections	217350
unique reflections	18990
completeness	95.6% (93.0%)
$I/\sigma(I)$	12.4 (7.3)
R_{merge}	0.056 (0.385)
Refinement Statistics	
R (%)	0.200
$R_{\text{free}}(\%)$	0.223
RMSD bonds (Å)	0.005
RMSD angles (°)	1.27
number of water atoms	121
$\langle B \rangle$ of protein atoms (Å ²)	19.0
$\langle B \rangle$ of inhibitor atoms (Å ²)	27.9
$\langle B \rangle$ of water atoms (Å ²)	22.7

contoured around 1.0, while the $F_{\text{obs}} - F_{\text{calc}}$ map was contoured at around 3.0 and around -3.0. The inhibitors were modeled considering the expected stereochemistry deduced from small-molecule structures. The models were found to fit the electron-density maps superbly. A refinement library has been constructed for this stereochemistry to restrain the refinement with CNS. Model building and crystallographic refinement was performed iteratively. When the inhibitor model was complete, it was included in the refinement with the restraint of the above-mentioned stereochemical library. The free R factor continued to fall through several further rounds of refinements. Final coordinates were analyzed using PROCHECK.²¹ The resulting electron density maps showed clear densities for most of the atoms including the bound inhibitor (Figure 5) except for a few side chains on the molecular surface. The final crystallographic and free R factors are 0.200 and 0.233, with reasonable stereochemistry (Table 1). All drawings for protein structure in the figures were generated using PyMOL.²¹ The coordinates have been deposited in the Protein Data Bank (access code 2RG3).

Mass Spectrometry. ESI spectra were acquired on a Q-TOF-2 (Micromass Ltd., Manchester, U.K.) hybrid mass spectrometer operated in MS mode and acquiring data with the time-of-flight analyzer. The instrument was operated for maximum sensitivity with all lenses optimized, while infusing a sample of lysozyme. The cone voltage was 35 eV and Ar was admitted to the collision cell and set to 20 V. Spectra were acquired at 11364 Hz pusher frequency covering the mass range 800 to 3000 amu and accumulating data for 6 s per cycle. Time mass calibration was made with CsI cluster ions acquired under the same conditions. Samples were desalted on a short column (3 mm × 1 mm ID) of reverse phase (RP) C18 resin (Zorbax, 5 μM, 300 Å). Samples were loaded onto the RP column from a 1% acetic acid solution with protein (5 μg), washed in the same, and eluted with 90% methanol and 0.5% formic acid directly into the ESI source. The resulting suite of charge states in the ESI spectrum were subjected to charge state deconvolution to present a “zero” charge mass spectrum using the Transform or MaxEnt 1 routine in MassLynxs software.

Enzyme Assays and Inhibition Studies. Progress Curve Method. The apparent second-order inactivation rate constants ($k_{\text{inact}}/K_1 \text{ M}^{-1} \text{ s}^{-1}$) were determined in duplicate. Typical progress curves for the hydrolysis of MeO-Suc-AAPV p-NA by HNE in the presence of inhibitor I are shown in Figure 2. The release of *p*-nitroaniline was monitored continuously at 410 nm. The pseudo first-order rate constant (k_{obs}) for the inhibition of HNE and PR 3 as a function of time was determined according to eq 1 below, where A is the absorbance at 410 nm, v_0 is the reaction velocity at $t = 0$, v_s is the final steady state velocity, k_{obs} is the observed first-order rate constant to steady state, and A_0 is the absorbance at $t = 0$. The k_{obs} values were obtained by fitting the $A \sim t$ data into eq 1 using nonlinear regression analysis (SigmaPlot, Jandel Scientific). The second order rate constants were determined by calculating

$k_{\text{obs}}/[I]$ and then correcting for the substrate concentration using eq 2. Control curves in the absence of inhibitor were linear.

$$A = v_s t + \{ (v_0 - v_s) (1 - e^{-k_{\text{obs}} t}) \} / k_{\text{obs}} + A_0 \quad (1)$$

$$k_{\text{inact}}/K_1 = (k_{\text{obs}}/[I]) (1 + [S]/K_m) \quad (2)$$

Acknowledgment. Support of this work by the Heart and Blood Institute of the National Institutes of Health (HL 57788 to W.C.G.), the National Center for Research Resources/National Institutes of Health (P20 RR 17708), KSTAR, NSF EPSCoR, and the University of Kansas, for the purchase of the Q-TOF-2 mass spectrometer, is gratefully acknowledged.

References

- 1) Silverman, R. B. Mechanism-Based Enzyme Inactivators. *Methods Enzymol.* **1995**, 249, 240–283.
- 2) (a) Churg, A.; Wright, J. L. Proteases and Emphysema. *Curr. Opin. Pulm. Med.* **2005**, 11, 153–159. (b) Barnes, P. J. Mediators of Chronic Obstructive Pulmonary Disease. *Pharmacol. Rev.* **2004**, 56, 515–548. (c) Barnes, P. J.; Stockley, R. A. COPD: Current Therapeutic Interventions and Future Approaches. *Eur. Respir. J.* **2005**, 25, 1984–1106. (d) Shapiro, S. D.; Ingenito, E. P. The Pathogenesis of COPD. *Am. J. Respir. Cell Mol. Biol.* **2005**, 32, 367–372. (e) Shapiro, S. D.; Goldstein, N. M.; Houghton, A. M.; Kobayashi, D. K.; Kelley, D.; Belaouaj, A. Neutrophil Elastase Contributes to Cigarette Smoke-Induced Emphysema in Mice. *Am. J. Pathol.* **2003**, 163, 2329–2335. (f) Rees, D. D.; Brain, J. D.; Wohl, M. E.; Humes, J. L.; Mumford, R. A. Inhibition of Neutrophil Elastase in CF Sputum by L-658,758. *J. Pharmacol. Exp. Ther.* **1997**, 283, 1201–1206. (g) Moraes, T. J.; Chow, C. W.; Downey, G. P. Proteases and Lung Injury. *Crit. Care Med.* **2003**, 31, S189–S194. (h) Balfour-Lynn, I. M. The Protease-Antiprotease Battle in the Cystic Fibrosis Lung. *J. R. Soc. Med.* **1999**, 92, S23–S30. (i) Van Der Geld, Y. M.; Limburg, P. C.; Kallenberg, C. G. Proteinase 3, Wegener's Autoantigen: From Gene to Antigen. *J. Leuk. Biol.* **2001**, 69, 177–190.
- 3) (a) Groutas, W. C.; Kuang, R.; Venkataraman, R.; Epp, J. B.; Ruan, S.; Prakash, O. Structure-Based Design of a General Class of Mechanism-Based Inhibitors of the Serine Proteinases Employing a Novel Amino Acid-Derived Heterocyclic Scaffold. *Biochemistry* **1997**, 36, 4739–4750. (b) Groutas, W. C.; Kuang, R.; Ruan, S.; Epp, J. B.; Venkataraman, R.; Truong, T. M. Potent and Specific Inhibition of Human Leukocyte Elastase, Cathepsin G and Proteinase 3 by Sulfone Derivatives Employing the 1,2,5-Thiadiazolidin-3-one 1,1-Dioxide Scaffold. *Bioorg. Med. Chem.* **1998**, 6, 661–671. (c) Kuang, R.; Venkataraman, R.; Ruan, S.; Groutas, W. C. Use of the 1,2,5-Thiadiazolidin-3-one 1,1-Dioxide and Isothiazolidin-3-one 1,1-Dioxide Scaffolds in the Design of Potent Inhibitors of Serine Proteinases. *Bioorg. Med. Chem. Lett.* **1998**, 8, 539–544. (d) Kuang, R.; Epp, J. B.; Ruan, S.; Chong, L. S.; Venkataraman, R.; Tu, J.; He, S.; Truong, T. M.; Groutas, W. C. Utilization of the 1,2,5-Thiadiazolidin-3-one 1,1-Dioxide Scaffold in the Design of Potent Inhibitors of Serine Proteinases: SAR Studies Using Carboxylates. *Bioorg. Med. Chem.* **2000**, 8, 1005–1016. (e) He, S.; Kuang, R.; Venkataraman, R.; Tu, J.; Truong, T. M.; Chan, H.-K.; Groutas, W. C. Potent Inhibition of Serine Proteinases by Heterocyclic Sulfide Derivatives of 1,2,5-Thiadiazolidin-3-one 1,1-Dioxide. *Bioorg. Med. Chem.* **2000**, 8, 1713–1717. (f) Wong, T.; Groutas, C. S.; Mohan, S.; Lai, Z.; Alliston, K. R.; Vu, N.; Schechter, N. M.; Groutas, W. C. 1,2,5-Thiadiazolidin-3-one 1,1-Dioxide-Based Heterocyclic Sulfides are Potent Inhibitors of Human Tryptase. *Arch. Biochem. Biophys.* **2005**, 436, 1–7. (g) Wei, L.; Lai, Z.; Gan, X.; Alliston, K. R.; Zhong, J.; Epp, J. B.; Tu, J.; Perera, A. B.; Van Sipdonk, M.; Groutas, W. C. Mechanism-Based Inactivation of Human Leukocyte Elastase via an Enzyme-Induced Sulfonamide Fragmentation Process. *Arch. Biochem. Biophys.* **2004**, 429, 60–70. (h) Lai, Z.; Gan, X.; Wei, L.; Alliston, K. R.; Yu, H.; Li, Y. H.; Groutas, W. C. Potent Inhibition of Human Leukocyte Elastase by 1,2,5-Thiadiazolidin-3-one 1,1-Dioxide-Based Sulfonamide Derivatives. *Arch. Biochem. Biophys.* **2004**, 429, 191–197.
- 4) Nomenclature used is that of Schechter, I.; Berger, A. *xx. Biochem. Biophys. Res. Commun.* **1967**, 27, 157–162, where $S_1, S_2, S_3, \dots, S_n$ and $S_1', S_2', S_3', \dots, S_n'$ correspond to the enzyme subsites on either side of the scissile bond. Each subsite accommodates a corresponding amino acid residue side chain designated $P_1, P_2, P_3, \dots, P_n$ and $P_1', P_2', P_3', \dots, P_n'$ of the substrate or (inhibitor). S_1 is the primary substrate specificity subsite, and $P_1 - P_1'$ is the scissile bond.
- 5) (a) Groutas, W. C.; Epp, J. B.; Kuang, R.; Ruan, S.; Chong, L. S.; Venkataraman, R.; Tu, J.; He, S.; Yu, H.; Fu, Q.; Li, Y.-H.; Truong, T. M.; Vu, N. T. 1,2,5-Thiadiazolidin-3-one 1,1-Dioxide: A Powerful

Scaffold for Probing the S' Subsites of (Chymo)trypsin-like Serine Proteases. *Arch. Biochem. Biophys.* **2001**, *385*, 162–169. (b) Groutas, W. C.; He, S.; Kuang, R.; Ruan, S.; Tu, J.; Chan, H-K. Inhibition of Serine Proteases by Functionalized Sulfonamides Coupled to the 1,2,5-Thiadiazolidin-3-one 1,1-Dioxide Scaffold. *Bioorg. Med. Chem.* **2001**, *9*, 1543–1548.

(6) Kuang, R.; Epp, J. B.; Ruan, S.; Yu, H.; Huang, P.; He, S.; Tu, J.; Schechter, N. M.; Turbov, J.; Froelich, C. J.; Groutas, W. C. A General Inhibitor Scaffold for Serine Proteases with a (Chymo)trypsin-like Fold: Solution-Phase Construction of the First Series of Libraries of Mechanism-Based Inhibitors. *J. Am. Chem. Soc.* **1999**, *121*, 8128–8129.

(7) (a) Abrahamson, D. R.; Irvin, M. H.; Blackburn, W. D.; Heck, L. W. Degradation of Basement Laminin by Human Neutrophil Elastase. *Am. J. Pathol.* **1990**, *136*, 1267–1274. (b) Kafienah, W.; Buttle, D.; Hollander, A. P. Cleavage of Native Type I Collagen by Human Neutrophil Elastase. *Biochem. J.* **1998**, *330*, 897–902. (c) Rao, N. V.; Wehner, N. G.; Marshall, B. C.; Gary, W. R.; Gray, B. H.; Hoidal, J. R. Characterization of Proteinase 3, A Neutrophil Serine Proteinase. Structural and Functional Properties. *J. Biol. Chem.* **1991**, *266*, 9540–9548.

(8) Bode, W.; Meyer, E.; Powers, J. C. Human Leukocyte Elastase and Porcine Pancreatic Elastase: X-ray Crystal Structures, Mechanism, Substrate Specificity, and Mechanism-Based Inhibition. *Biochemistry* **1989**, *28*, 1951–1963.

(9) Fujinaga, M.; Chenaia, M. M.; Halenbeck, R.; Koths, K.; James, M. N. G. The Crystal Structure of PR 3, A Neutrophil Serine Proteinase Antigen of Wegener's Granulomatosis Antibodies. *J. Mol. Biol.* **1996**, *261*, 267–278.

(10) Brubaker, M. J.; Groutas, W. C.; Hoidal, J. R.; Rao, N. V. Human Neutrophil Proteinase 3: Mapping of the Substrate Binding Site Using Peptidyl Thiobenzyl Esters. *Biochem. Biophys. Res. Comm.* **1992**, *188*, 1318–1324.

(11) Kam, C. M.; Kerrigan, J. E.; Dolman, K. M.; Goldschmeding, R.; Von dem Borne, A. E.; Powers, J. C. Substrate and Inhibitor Studies on Proteinase 3. *FEBS Lett.* **1992**, *297*, 119–123.

(12) Korkmaz, B.; Knight, G.; Bieth, J. Compared Action of Neutrophil Proteinase 3 and Elastase on Model Substrates. Favorable Effect of S'–P' Interactions on Proteinase 3 Catalysis. *J. Biol. Chem.* **2003**, *278*, 12609–12612.

(13) Hajjar, E.; Korkmaz, B.; Gautheir, F.; Brandsdal, B. O.; Witko-Sarsat, V.; Reuter, N. Inspection of the Binding Sites of Proteinase 3 for the Design of a Highly Specific Substrate. *J. Med. Chem.* **2006**, *49*, 1248–1260.

(14) (a) Morrison, J. F.; Walsh, C. T. The Behaviour and Significance of Slow Binding Inhibitors. *Adv. Enzymol.* **1988**, *61*, 201–301. (b) Wakselman, M.; Xie, J.; Mazaleyrat, J. P. New Mechanism-Based Inhibitors of Trypsin-like Proteinases. Selective Inhibition of Urokinase by Functionalized Cyclopeptides Incorporating a Sulfonomethyl-Substituted m-Aminobenzoic Acid. *J. Med. Chem.* **1993**, *36*, 1539–1547. (c) Weir, M. P.; Bethell, S. S.; Cleasby, A.; Campbell, C. J.; Dennis, R. J.; Dix, C. J.; Finch, H.; Jhoti, H.; Mooney, C. J.; Patel, S.; Tang, C-M.; Ward, M.; Wonacott, A. J.; Wharton, C. W. Novel Natural Product 5,5-trans-Lactone Inhibitors of Human alpha-Thrombin: Mechanism of Action and Structural Studies. *Biochemistry* **1998**, *37*, 6645–6657. (d) Copeland, R. A. Evaluation of Enzyme Inhibitors. In *Drug Discovery*; Wiley: New York, 2005.

(15) (a) Abbenante, G.; Fairlie, D. P. Protease Inhibitors in the Clinic. *Med. Chem.* **2005**, *1*, 71–104. (b) Edwards, P. D. In *Proteinase and Peptidase Inhibition*; Smith, H. J., Simons, C., Eds.; Taylor and Francis: London, 2002.

(16) (a) Nakayama, Y.; Odakagi, Y.; Fujita, S.; Matsuoka, S.; Kamanaka, N.; Nakai, H.; Toda, M. Clarification of the Mechanism of Human Sputum Elastase Inhibition by a New Inhibitor, ONO-5046, Using Electrospray Ionization Mass Spectrometry. *Bioorg. Med. Chem.* **2002**, *12*, 2349–2353. (b) Knight, W. B.; Swiderek, K. M.; Sakuma, T.; Calaycay, J.; Shively, J. E.; Lee, T. D.; Covey, T. R.; Shushan, B.; Green, B. G.; Chabin, R.; Shah, S.; Mumford, R.; Dickinson, T. A.; Griffin, P. R. Electrospray Ionization Mass Spectrometry as a Mechanistic Tool: Mass of Human Leukocyte Elastase and a β -Lactam-Derived E-I Complex. *Biochemistry* **1993**, *32*, 2031–2035.

(17) Otwinowski, Z.; Minor, W. Processing of X-ray Diffraction Data Collected in Oscillation Mode. *Methods Enzymol.* **1997**, *276*, 307–326.

(18) Read, R. J. Pushing the Boundaries of Molecular Replacement with Maximum Likelihood. *Acta Crystallogr.* **2001**, *D57*, 1373–1382.

(19) Jones, T. A.; Zhou, J. Y.; Cowan, S. W.; Kjelgaard, M. Improved Methods for Building Protein Models in Electron Density Maps and the Location of Errors in These Models. *Acta Crystallogr.* **1991**, *47*, 110–119.

(20) Brünger, A. T.; Adams, P. D.; Clore, G. M.; Delano, W. L.; Gros, P.; Grossesse-Kunstleve, R. W. Crystallography and NMR System: A New Software Suite for Macromolecular Structure determination. *Acta Crystallogr.* **1998**, *54*, 905–921.

(21) DeLano, W. L. The PyMOL Molecular Visualization System. <http://www.pymol.org>, 2002.

JM700966P